BNL 7309

DYNAMICS OF RADIATION DAMAGE IN A BODY-CENTERED CUBIC LATTICE*

C. Erginsoy, G. H. Vineyard, and A. Englert-Chwoles†

Brookhaven National Laboratory, Upton, N. Y.

* Work supported by the U. S. Atomic Energy Commission.

† Permanent address: European Research Associates, Brussels, Belgium.

DISCLAIMER

ABSTRACT

Radiation damage has been studied by numerically integrating the equations of motion of a large set of atoms on a high speed computer. In this paper the method is applied to a model of α-iron. Low energy events have been extensively investigated. The primary knock-on atom is found to initiate an extended sequence of correlated replacements, producing an interstitial at some distance and a vacancy on its original site. The interstitial is found to have a split configuration, as was found earlier in copper, but its axis lies along $\langle 110 \rangle$. Collision chains are found to be prominent in $\langle 111 \rangle$ and $\langle 100 \rangle$, and attenuation rates and focusing parameters for these chains are determined. The threshold energy for displacing an atom is found to be highly dependent on the direction of the knock-on. The lowest threshold is found to be 17 eV, for knock-ons directed near $\langle 100 \rangle$, and to be about 34 eV and 38 eV for those directed near $\langle 110 \rangle$ and $\langle 111 \rangle$, respectively. The probability of displacement for a randomly directed knock-on of energy E is determined for E between 0 and 60 eV. The results are in approximate agreement with experiments of Lucasson and Walker, although more structure is found in the calculated curve than could be tested by the experiments. Pronounced directional effects in low-energy electron bombardments of α-iron single crystals are predicted.

1. INTRODUCTION

The processes by which radiation damage is produced in a crystal have recently been investigated by a new method in which the classical equations of motion of a set of several hundred to a thousand atoms are integrated on a high speed computer. The atoms are allowed to interact with fairly realistic central forces, augmented by special forces on the atoms at the edge of the set designed to simulate the influence of surrounding material. Initially the atoms are at rest on the sites of a perfect lattice, and the start of a radiation damage even is considered to be the sudden transfer of momentum to one of the atoms (the primary knock-on) by an irradiating particle. The primary knock-on then energizes other atoms in a complex many-body process, and when the agitation dies away the model crystallite is left in a damaged state. Since the primary knock-on may have any momentum, within wide limits, a series of calculations for representative initial conditions must be made. No presuppositions about the nature of the lattice defects, or about thresholds for their production, are made -- such information is an end product of the calculations. The chief assumption which must be made is the form of the interatomic potential energy, and a number of experimental and theoretical requirements are imposed on this. Also, an upper limit on the energy of the primary knock-on is imposed by the size of the set of atoms.

The first calculations of this kind were made on a model representing copper.[1-7] A large number of calculations were made and the production of interstitials and vacancies was "observed". Threshold energies for the principal crystallographic directions were computed. Correlated collision chains along ⟨100⟩ and ⟨110⟩ were found to be prominent, and numerous re-

placements were found to occur for each lattice defect that was made. Configurations and properties of a number of elementary lattice defects were investigated in the same model by an extension of the computational techniques. A very few calculations have also been made[9] in a simple model or ordered Cu_3Au. In spite of the disparity of masses, sequences or replacement collisions which produce large amounts of disorder were found.

As the next system for investigation we have chosen α-iron[8,9]. It was desired to have a representative of another lattice, and the body-centered cubic lattice of α-iron, while still simple, was thought to present interesting differences from the face-centered cubic lattice of copper. A further reason for choosing iron was the fact that some recent experimental radiation damage studies had been made on it with electrons,[10] and, of course, a wealth of information on its various physical properties exists. The force law employed in the model has been refined to give good agreement with the experimental radiation damage threshold, as well as to meet other requirements described in Section 2.

Some static calculations were carried out in order to determine more closely the configurations of the stable lattice defects observed in the dynamic runs. The interstitial was found to have a new split configuration. Section 3 describes the static results.

Over one-hundred dynamic events were run with different starting conditions of knock-on energy and initial direction. One of the principal objects of the calculations was to obtain the threshold energy of displacement for a large variety of initial directions and to derive the displacement probability for a knock-on of given energy and random direction. It was also expected that as a result of analyzing a large number of near-threshold dynamic events, more insight could be gained into the displacement

processes themselves, especially regarding the many-body features and directional effects. The highest knock-on energy used in this systematic survey was 60 eV. A number of higher energy runs were also made in some selected directions. Detailed results are given and discussed in Section 4. A summary of the conclusions follows in Section 5.

2. THE MODEL

Calculations have been performed on sets of N atoms interacting with pairwise central forces and supplemented by special "surface" forces on the atoms near the boundary of the set. The surface forces consist of a constant force, a spring force (proportional to the displacement of an atom from its lattice site) and a viscous force (proportional to minus the velocity of an atom). The constant force is chosen such that the set can be in static equilibrium on the sites of a body-centered cubic lattice. The spring and viscous forces approximate the reaction to displacements that would be provided by atoms outside the set of N if the set were imbedded in any infinite crystal. The method of choosing the spring and viscous force constants is essentially the same as was used in the model of copper, described in reference 1. The spring forces were chosen by considerations of an equivalent elastic continuum, and simulate the response of the surroundings of the set to static distortions of the set. The viscous force constants were chosen by consideration of the best impedance match for plane elastic waves incident upon an infinite plane boundary, and allow energy to disappear from the set of N atoms, so that a quiescent state is eventually reached. It should be

noted that these boundary conditions are quite different from the periodic boundary conditions employed in certain statistical mechanical calculations[11] which have a superficial resemblance to ours.

In the f.c.c. lattice it was possible to cut off the pairwise potential at a distance somewhat less than the second neighbor spacing, so that, at equilibrium, only nearest neighbors were interacting. On the other hand, the b.c.c. lattice is unstable with only nearest neighbor central forces, and thus in the present calculations the pairwise interaction potential was taken into account through second neighbors. Equilibration then demanded that a constant force be applied on the first layer of atoms beneath the surface as well as on the surface layer itself. A weak spring force was applied to the layer beneath the surface as well as to the surface layer, but, for simplicity, and because no physical distinction was expected, the viscous force was applied to the surface layer alone. The spring force constants on the layer beneath the surface were chosen, somewhat arbitrarily, to be about one two hundredth as large as those on the surface layer.

Most of the calculations reported here, including all events near threshold, were done with a cubic set measuring 14 x 14 x 14, where the unit of length is one-half the edge of the cubic unit cell, containing 855 atoms. Some events in which the primary knock-on was directed near ⟨100⟩ were calculated in a set measuring 26 x 10 x 10 and containing 829 atoms. The imperfect treatment of surface and near-surface atoms was believed to be a very minor disturbance in the events reported, because calculations were always arranged to keep the displacements of surface atoms small and to have the regions of important dynamic action in the interior of the set.

The pairwise interaction potential $\varphi(\underline{r})$ was chosen with considerable care. Three potentials (denoted by Roman numerals hereafter and shown in Figs. 1 and 2) were tried, and, for reasons to be explained, potential III was deemed most realistic and the bulk of the calculations were done with it. Potential I is a Born-Mayer potential of the form

$$\varphi(\underline{r}) = 2570\ e^{-2.095\underline{r}} \tag{1}$$

where $\varphi(\underline{r})$ is in electron volts and $\underline{r}$ is in units of one-half the cube edge (1.43 Å). This potential gave a threshold for production of permanent damage by a ⟨100⟩ knock-on considerably above 35 eV. Since ⟨100⟩ proves to be the easiest direction for the production of damage and since the experimental threshold is around 18 eV in iron,[10] Potential I is too stiff and was abandoned.

Potential II is a Morse potential with parameters derived by Girifalco and Weizer[12] to give good agreement with the cohesive energy and the compressibility of α-iron. The potential has the form

$$\varphi(\underline{r}) = D\left[\ e^{-2\alpha(\underline{r}-\underline{r}')} - 2e^{-\alpha(\underline{r}-\underline{r}')}\right] \tag{2}$$

where

$$D = 0.4174 \text{ eV}$$

$$\alpha = 1.3885 \text{ Å}^{-1}$$

$$\underline{r}' = 2.845 \text{ Å}$$

Figure 1 shows Potential II extrapolated to much smaller separations than its method of derivation warrants. This potential also gave too high a value for the displacement threshold energy and was used only for a few calculations[13] on the dynamics of replacement chains to show the effects of a high but soft potential.

Potential III is the one finally chosen for detailed work in the α-iron model. As can be seen in Fig. 2 it is repulsive for nearest neighbors (separation $\underline{r}_o$) and weakly attractive for second neighbors (separation $\underline{a}$). Potential III is a composite which meets a number of major requirements: In conjunction with the surface forces it gives a stable b.c.c. lattice of the right lattice constant; it gives good values for the three first-order elastic moduli; at small distances it joins the Thomas-Fermi (Firsov)[14] and the Thomas-Fermi-Dirac (Abrahamson)[15,16] potentials theoretically derived on the basis of the statistical atoms; finally, it gives the correct threshold energy for radiation damage.

Specifically, Potential III was chosen as follows. For $\underline{r} < 0.7$ it is an exponentially screened Coulomb potential given by

$$\varphi(\underline{r}) = \left(\frac{0.7}{\underline{r}}\right) 8573\, e^{-6.547\,\underline{r}} \tag{3}$$

This form, as is seen in Fig. 1, joins the statistical atom potentials at small $\underline{r}$ with good accuracy.

For $0.7 < \underline{r} < 1.35$ the potential is given by

$$\varphi(\underline{r}) = 8573\, e^{-6.547\,\underline{r}} \tag{4}$$

This Born-Mayer potential interpolates between the small $\underline{r}$ region and intermediate $\underline{r}$ region at which a Morse potential is used, and includes the region which determines the threshold displacement energy.

For $1.35 < \underline{r} < 2.0$, $\varphi(r)$ is given by the Morse potential of Eq. (2), except for the parameter D, which now has the value D = 0.223 eV (The parameters of the Born-Mayer potential in Eq. (4) were chosen to match this potential in value and slope at $\underline{r} = 1.35$.) Using this form of $\varphi(\underline{r})$, ex-

tended only through second neighbors, and the formulas for the elastic constants

$$c_{11} = \frac{2}{3\underline{r}_2}\left[\frac{2}{\underline{r}_1}\varphi'(\underline{r}_1) + \varphi''(\underline{r}_1) + 3\varphi''(\underline{r}_2)\right], \tag{5a}$$

$$c_{12} = \frac{2}{3\underline{r}_2}\left[-\frac{4}{\underline{r}_1}\varphi'(\underline{r}_1) + \varphi''(\underline{r}_1) - \frac{3}{\underline{r}_2}\varphi'(\underline{r}_2)\right], \tag{5b}$$

$$c_{44} = \frac{2}{3\underline{r}_2}\left[\frac{2}{\underline{r}_1}\varphi'(\underline{r}_1) + \varphi''(\underline{r}_1) + \frac{3}{\underline{r}_2}\varphi'(\underline{r}_2)\right], \tag{5c}$$

where $\underline{r}_1$ and $\underline{r}_2$ are the nearest and second neighbor separations, respectively, exact agreement with the experimental bulk modulus and fairly good agreement with the other experimental elastic constants is obtained, as shown in Table 1.

Table 1. Comparison of Elastic Constants for α-iron (units 10^{11} dynes/cm^2)

	c_{11}	c_{12}	c_{44}	$B = (1/3)(c_{11} + 2c_{12})$
Experimental	23.7	14.1	11.6	17.3
Calculated with Potential III	19.2	16.4	10.4	17.3

Since the surface pressure represents some part of the binding provided by the conduction electrons, it might be expected to make a further contribution to the elastic constants. This effect has been omitted, however, from the calculated values in Table 1.

For $2.0 < \underline{r} < 2.5$, $\varphi(\underline{r})$ is taken to be the modified Morse potential multiplied by an arbitrarily chosen function of $\underline{r}$ which is equal to 1 at $\underline{r} = 2.0$ and diminishes smoothly to 0.1 at $\underline{r} = 2.5$. This makes $\varphi(2.5) = -0.014$ eV. For $r > 2.5$, $\varphi(\underline{r})$ is set equal to zero. The small discontinuity at this cut-off separation (shown as $\underline{r}_c$ in Fig. 2) does not affect the results of the calculations. The smooth reduction of $\varphi(\underline{r})$ from second neighbor separation to cut-off was found necessary if interactions of higher order neighbors was to be left out of account in a consistent way.

The computations were performed on IBM 7090 and IBM 7094 computers. The integration methods were the same as described in reference 1, and the same checks and precautions were observed.

In some highly directionalized events such as collision chains, in which almost all of the action was localized in a few atoms at a time, a new technique, called "Leap Frog", was used to follow the action beyond the boundaries of the set. By this technique, displacements and velocities of a restricted group of atoms near the right edge of our fundamental set could, at a selected instant, be automatically made the starting displacements and velocities of a similar group near the left edge of a second fundamental set. Iteration of the process gave a set which was, effectively, indefinitely extended in one dimension.

3. STATIC CALCULATIONS

A number of static calculations have been carried out in order to determine, in our model, the configuration of the simple defects (vacancy and interstitial) and the stability of Frenkel pairs with different orientations and separations in the lattice. In these calculations a rough

estimate was first made of the defect configuration, and atoms were given these coordinates at the beginning. The machine program for solving the equations of motion of all the atoms in the set was then initiated and continued for a sufficient number of time steps until the equilibrium configuration was reached. As in the f.c.c. case (reference 1) an artificial damping scheme was used that set the kinetic energies of all the atoms to zero each time the total kinetic energy in the system reached a maximum. In this manner, long oscillations around the equilibrium configuration could be avoided and approximate equilibration could be achieved rather quickly. Unless otherwise stated, all calculations reported were made with Potential III. Energies and volumes of formation and migration of defects are not reported here.

The nearest neighbors around a vacancy were found to relax inward by about 6% of the equilibrium distance, $\sqrt{3}$. The second neighbors relaxed slightly outward.

The interstitial was found to have a split configuration, with its axis in the $\langle 110 \rangle$ direction. This was first established and reported[9] for our α-iron model with Potential II. Subsequent calculations with Potential III have given the same results. The configuration is reminiscent of the split interstitial found in the f.c.c. case,[1] except that the orientation in the latter was $\langle 100 \rangle$.

Figure 3 shows the equilibrium configuration of the interstitial in its $\{110\}$ plane. Dotted spheres refer to the original lattice sites and the solid spheres to the actual relaxed positions of the atoms. The two atoms forming the split interstitial (shown as I_A and I_B) are separated by a distance of approximately 0.72 (in units where the cube edge is 2.0) from the vacant site 0. The relaxation of the neighbors in the $\langle 111 \rangle$ directions,

which share the greatest part of the strain field, was found to be quite large, about 0.29 for atoms E, N, M and F, about 0.14 for atoms D, P, L, and G, and about 0.08 for atoms C, Q, K, and H.

Calculations on the stability of a Frenkel pair were carried out by setting up the interstitial configuration first. One of the lattice sites in the neighborhood of the interstitial was then vacated and calculations were run with these starting conditions. All close pairs were found to be unstable against recombination, whatever the orientation of the line joining the vacancy and the center of mass of the interstitial. If this line was a close packed ⟨111⟩ direction the minimum separation of the stable pair was particularly large. For instance a vacancy at C, Q, K or H in Fig. 3 was found to give an unstable pair with the split interstitial at I_A, I_B. All second neighbors of the vacant site 0 were also unstable against recombination. This strong dependence of the minimum separation of a stable Frenkel pair on orientation is very similar to that observed in the f.c.c. case.[1]

4. DYNAMIC RESULTS

A. General Remarks

Over one-hundred dynamic events were run with different starting conditions. Detailed descriptions of all these will not be given since the general picture was found to be quite similar to that discussed in reference 1 for the f.c.c. case. First, the existence of a clearly defined threshold energy for displacement was confirmed. Calculations have shown that for any knock-on direction there is a minimum kinetic energy which must be imparted to the knock-on so that it does not return to its original site. This is the threshold energy for displacing the atom in that direction.

The knock-on itself, however, was in no case found to go into an interstitial position. Invariably it was found to replace one of its neighbors. For energies up to 60-65 eV this replacement took place at the nearest neighbor, the second neighbor, or the third neighbor depending on the initial direction of the knock-on. It was found, further, that a more or less extended sequence of replacements accompanies this initial replacement, so that the eventual interstitial is formed several sites away from the vacancy left behind by the knock-on. The static calculations on the configuration of the split interstitial and the stability of a Frenkel pair, discussed in Section 3, confirm this picture.

A small selection of dynamic events with different starting conditions will now be discussed. Figures 4 and 5 show two dynamic events in which $\langle 100 \rangle$ and $\langle 111 \rangle$ replacement chains are operative, respectively. In Fig. 4 the knock-on (at 0) is directed at 25° to [100] in the (001) plane. It makes a replacement at C (third neighbor) and a replacement chain proceeds in the [010] direction. A vacancy is created at 0. The interstitial is not seen, as it will be formed beyond G. In Fig. 5 the knock-on makes a replacement at A' (second neighbor) and a focused replacement chain is seen in the $[\bar{1}\bar{1}1]$ direction. A vacancy is created at 0 and the interstitial is expected to form beyond D.

In a small range of directions it has been found that di-vacancies can be formed too. Figure 6 shows such an event at 70 eV. The knock-on makes a replacement at C (third neighbor) after displacing atom B (nearest neighbor). Two vacancies are created (at 0 and B) next to one another. One interstitial is seen at D, the other is expected to form beyond E.

B. Collision Chains

Figure 7 shows the ⟨111⟩, ⟨100⟩ and ⟨110⟩ directions in a b.c.c. lattice. The knock-on (K) can dynamically replace the first struck atom (S_1), producing a replacement chain which can proceed along one of the crystal axes. In the close-packed, ⟨111⟩, direction, K, in order to make a replacement, has to go through two "barrier" planes, one formed by the atoms A_1, A_2, A_3, and the other by the atoms B_1, B_2, B_3. The loss of energy from K to these atoms is found to be less than 1 eV, but the successive close-packed bonds KS_1 and S_1S_2 absorb considerable potential energy which the knock-on has to supply in order to make a replacement at S_1. It turns out, in fact, that the ⟨111⟩ is the hardest of the three main crystal axes for making a replacement and hence for creating a stable defect.

In the ⟨100⟩ direction, there is only one barrier plane, formed by $A_1A_2A_3A_4$, but this barrier absorbs a good deal more energy (5-6 eV) from K. On the other hand the KS_1 bond does not absorb as much potential as the corresponding close-packed bond in the ⟨111⟩ direction, since it is more open. Furthermore, the same four atoms which oppose the motion of K help to push K forward once it clears the halfway mark. This is a characteristic of the ⟨100⟩ threshold, which we find to be the lowest of all the three main crystal directions.

In the ⟨110⟩ direction, the barrier is highly asymmetrical, since A_1A_2 is equal to $\underline{a}$, the cube edge, while A_3A_4 is $\sqrt{2}\,\underline{a}$. The barrier is, therefore, particularly strong in the {110} plane.

As might be expected from the geometrical conditions described above, collision chains formed in the close-packed, ⟨111⟩, direction show a small energy loss at each step and, therefore, transfer kinetic energy

over large distances in the crystal. In the hard-sphere model these correspond to Silsbee's focused chains.[17] Figure 8 shows the time-dependence of the kinetic energy in such chains. The initial energy loss from K to S_1 should be noted; it is the loss that provides the potential energy needed to establish the chain. The rate of loss of energy thereafter is more or less constant. In the 55 eV case (upper curve) the pulse reaches the 50th struck atom and, therefore, covers a distance of 125 Å in 7×10^{-13} sec. This corresponds to a mean velocity of 1.8×10^6 cm/sec, something like 4 to 5 times the velocity of sound. One can consider this motion to be a kind of shock-wave whose velocity will gradually decrease as its amplitude decreases. The attenuation is expected to increase sharply when the pulse velocities become comparable to the velocity of sound. By the time the pulse will come to an end, therefore, it will have carried energy to a distance of $\sim$ 150 Å. At this point the energy in the pulse will have dropped to the order of the bond energies. The velocity of the 35 eV pulse shown in the lower curve is only slightly lower: the pulse starts with 1.7×10^6 cm/sec and slows down to 1.3×10^6 cm/sec when it reaches the 30th struck atom. This velocity is still 2-3 times the velocity of sound.

Pulses initially started at some angle to the ⟨111⟩ direction have also been studied. Table 2 shows that the attenuation becomes larger and the average pulse velocity v becomes somewhat lower as the initial angle to the ⟨111⟩ increases.

TABLE 2

Maximum Kinetic Energies (eV) Transferred to Successive Atoms and the Average Pulse Velocity v (10^6 cm/sec) in ⟨111⟩ Collision Chains

E_o	Initial angle to ⟨111⟩	E_1	E_2	E_3	E_4	E_5	E_6	E_7	E_8	v
40.0	4.75°	31.9	29.6	27.3	25.4	23.5	21.6	20.0	18.7	1.7
39.0	7.25°	29.8	26.1	23.2	20.5	18.1	16.2	14.7	13.5	1.6
39.0	10.75°	18.5	10.1	6.2	4.5	3.5	2.8	2.1	1.5	1.1

Figure 9 shows that in ⟨100⟩ directions pulse velocities are lower and the drag is greater. A 40 eV pulse was found to be attenuated completely within 10 atomic distances. This is consistent with other dynamic results which indicate that the defects formed by ⟨100⟩ chains are closer to their vacancies than those formed by ⟨111⟩ pulses of equal energy. The effects of thermal vibrations on the lengths of these chains remain to be studied.

In the ⟨110⟩ direction energy losses are still greater for each step in the replacement sequence. Figure 10 shows a replacement sequence initiated by a 100 eV knock-on at 1° to [110] in the (001) plane. Successive replacement collisions are clearly correlated. They start initially in [110] and defocusing causes a change in direction to a [010] sequence. The kinetic energies transerred to successive replaced atoms in this sequence were calculated to be 73.4 eV to atom A, 49.7 eV to atom B, and 18.2 eV to atom C. The interstitial is seen in Fig. 10 to be forming around the site E.

As in the f.c.c. case, there is a strong tendency of energy to propagate along two preferred directions; in the b.c.c. case these are the close-packed ⟨111⟩

and the cubic ⟨100⟩ directions. The focusing parameters $\Lambda(E)$ associated with these two directions have been studied. A collision chain was characterized in the $\underline{i}$th stage ($\underline{i} = 1,2,3,\ldots$) by an energy E_i (the kinetic energy of the atom at the point of its maximum kinetic energy) and an angle θ_i (angle between the axis of the chain and the velocity vector of the moving atom at its point of maximum kinetic energy). If the angle at the next stage is θ_{i+1} the focusing parameter at the stage $\underline{i}$ is defined as

$$\Lambda(E_i) = \theta_{i+1}/\theta_i \tag{6}$$

The values of $\Lambda(E)$ for a variety of energies E and angles θ below 10^o have been calculated and plotted against E in Fig. 11 for ⟨111⟩ and in Fig. 12 for ⟨100⟩ chains. As in the f.c.c. case (reference 1) very little dependence of Λ on θ was observed. The energy below which a ⟨111⟩ chain focuses is seen in Fig. 11 to be about 28 eV. According to the hard-sphere picture this energy should be $2V(\sqrt{3}/2)$ or 59 eV for our potential. Obviously the hard-sphere model overestimates the focusing for such a potential. In Fig. 12 the focusing parameter of ⟨100⟩ chains within the b.c.c. lattice is shown, together with that of an isolated row having the same spacing as a ⟨100⟩ row and interacting with the same potential. It has been suggested recently[18] that the focusing mechanism in the ⟨100⟩ direction for a b.c.c. lattice should be independent of the action of the neighboring atoms, i.e., governed purely by the Silsbee mechanism. Figure 12 indicates, however, that an isolated row exhibits practically no focusing and that the observed focusing must, therefore, be attributed to the action of the neighbors forming the barrier plane $A_1A_2A_3A_4$ of Fig. 7. In this case too, focusing

is not as strong as that predicted by a hard-sphere model. The limiting energy for focusing is seen in Fig. 12 to be about 18 eV, whereas the hard-sphere picture predicts an energy equal to 2V(1) = 24.6 eV.

C. Directional Dependence of Displacement Threshold

In the simplest model of radiation damage (hard-spheres in a random assembly), a constant threshold energy E_d has customarily been assumed. Obviously the displacement threshold will depend on the direction of motion of the primary knock-on, and a random distribution of directions will give rise to a displacement probability $P_d(E)$ which will start up from zero at a minimum threshold (the threshold in the easiest direction) and reach unity at some higher energy. Refined calculations of radiation damage have employed the function $P_d(E)$ but have had to make arbitrary assumptions as to its form. It was of interest, therefore, to calculate the threshold for each direction in the present model, which includes directional and many-body effects without arbitrary assumptions, and from this to derive $P_d(E)$.

In Fig. 13 a spherical triangle is shown that contains all the non-equivalent direction for the knock-on. In the present calculations, the three edges of the triangle were systematically investigated, as well as a number of directions on the interior of the triangle. For each direction the threshold was estimated by finding two energies, the higher of which gave a stable replacement and the lower of which did not.

It was found that at low energies the replacement by the knock-on follows a very simple pattern: the knock-on replaces a nearest neighbor, a second neighbor or a third neighbor depending on whether its original direction is closer to a ⟨111⟩, a ⟨100⟩ or a ⟨110⟩ axis. This pattern is

shown schematically in Fig. 13. It is interesting to note that in no case is the knock-on able to escape the sphere of radius 4.05 Å centered on it and containing the 12 third neighbors. At higher energies (above 70 eV) the knock-on was found to replace the 4th, 5th, etc. neighbor, if it was directed in an "internal" direction between the main crystal axes.

Figure 14 shows the directional dependence of the displacement threshold energy in the two planes (001) and $(1\bar{1}0)$. The direction of easiest displacement is seen to be [100], giving a minimum threshold of $\sim$ 17 eV in our model with Potential III. The local minima in the vicinity of [110] and [111] are $\sim$ 34 eV and $\sim$ 38 eV, respectively. It will be noted that in each general direction the threshold is a minimum when the knock-on is directed a few degrees off the axis. The [100] does not show this effect to any significant degree, while it is rather pronounced in the [110] and especially pronounced in the [111] direction. This is because replacements are energetically easier with a small degree of defocusing. The range of initial directions in which the replacement is in the ⟨111⟩ direction is seen from Fig. 13 to be large and to be symmetrical around the axis. The same is true of the ⟨100⟩, but the range of directions around ⟨110⟩ is severely restricted in the {110} plane. The knock-on has to be directed very close to ⟨110⟩ in order to make a replacement in that direction. Note also that in intermediate directions between two crystal axes the threshold rises sharply, as the knock-on is losing energy to two repulsive bonds at the same time. In a small range of directions the knock-on is unable to make a final replacement in either of the two directions and returns to its site. In such directions the threshold is limited by another type of replacement (to the 4th neighbor, 5th neighbor, etc.) at higher energies. These

events have not been shown in Fig. 14, where the knock-on energy has been limited to 60 eV.

Figure 15 shows the displacement threshold contours over the stereographic triangle. The integrated probability $P_d(E)$ of displacement as a function of knock-on energy, for a randomly directed knock-on, is shown in Fig. 16. The integration has been carried out numerically by taking into account the contours of threshold in different directions and using the symmetry properties of the lattice. The probability at each energy equals the sum of solid angles in which a knock-on of that energy makes a stable replacement, divided by 4π. The "two step" nature of the curve will be noted. The individual contributions of the different directions have been shown separately. A striking feature of the curve is that, whereas the lowest threshold in the easiest direction is 17 eV, the probability rises rather slowly with energy. The probability reaches 0.5 at $E \sim 40$ eV and at $E = 60$ eV (limit for the detailed calculations reported in this paper) the probability is only 0.76.

This slow increase of the displacement probability with energy may explain the persistent discrepancy between the number of defects estimated on the basis of a sharp threshold at ~ 25 eV and the experimental results of low-temperature electron bombardment. Lucasson and Walker[19] have carried out such measurements with iron. The best fit for their results corresponded to a "staircase function"[20] for the displacement probability. This function is shown in Fig. 16 for comparison with our calculated curve. It should be noted that the lowest electron energy they used was 600 keV, so that the comparison should be made only for knock-on energies above ~ 35 eV. With this restriction there is reasonable agreement between the curves. Both show an extended region between 40-60 eV where P_d lies between 0.6 and 0.8. It remains to be seen whether electron-bombardment

with lower energy beams ($\sim$ 300 keV) on oriented single crystals of α-iron will show the lower energy step which these calculations predict. If the predicted effect exists it should be possible to observe a large difference in the damage rates in a $\langle 111 \rangle$-oriented crystal and in a $\langle 100 \rangle$-oriented crystal under the same electron bombardment conditions. Such an experiment would provide an important test to the interatomic potential assumed, and an experimentally obtained curve of $P_d(E)$ vs. E could help to determine the potential more accurately in the range of intermediate separations.

5. CONCLUSIONS

To the extent that the interatomic potentials at the separations of interest to radiation damage processes can be accurately simulated by two-body central forces, dynamic calculations by means of a large capacity digital computer can give a good account of the details of the displacement processes. This was first established in the case of the f.c.c. lattice,[1] using copper as a model, and the present calculations show that the case of a b.c.c. lattice is qualitatively similar.

The following conclusions can be drawn from the present calculations on the model of α-iron:

1) The key mechanism of displacement at low energies is a dynamic replacement by the knock-on. The knock-on itself does not go into an interstitial configuration but replaces one of its neighbors. At threshold energies this can be a nearest neighbor, a second neighbor or a third neighbor depending on the initial knock-on direction. Higher order neighbors can be replaced only at energies higher than about 70 eV and for knock-on directions between the main low-index directions. A

replacement by the knock-on causes a more or less extended sequence of correlated replacements, and the interstitial is formed several atomic distances from the vacancy. Such a sequence is probably the most important mechanism in separating the interstitial from the vacancy.

2) The stable form of the interstitial in the b.c.c. lattice is found to be a split configuration oriented along ⟨110⟩. Both potentials II and III lead to this result. In the previous calculations on copper[1] the interstitial was also found to be split, but was oriented in ⟨100⟩.

3) As in the calculations for an f.c.c. lattice (copper) Frenkel pairs are unstable against recombination when they are closely spaced. The minimum separation for stability is highly dependent on the orientation of the line joining the vacancy and the center of mass of the split interstitial. This minimum separation is largest for a pair in which this line is a ⟨111⟩(close-packed) direction. All close Frenkel pairs were found to be unstable.

4) Collision chains are found to be prominent in ⟨111⟩ and ⟨100⟩ at threshold energies. Sequences in ⟨110⟩ can also be established at about 100 eV. All collision chains propagate with supersonic velocities and may be considered as sharply pointed shock waves. Chains in ⟨111⟩ have the lowest rate of energy loss and the greatest range. The effects of lattice vibrations on the range of the chains have not yet been examined, but small angular deviations in the original direction of motion of the knock-on have a relatively small influence on the velocity of the pulse.

5) The threshold energy for displacing an atom is highly dependent on direction. In the b.c.c. lattice the direction of easiest displacement is near ⟨100⟩ (estimated threshold 17 eV for Potential III). The thresholds for ⟨110⟩ and ⟨111⟩ are about 34 eV and 38 eV, respectively.

The details of the replacement process are different for each direction, since they depend on the barriers formed by neighboring atoms. The minimum threshold associated with each of the above direction occurs a few degrees off the axis. The thresholds exactly along the axes are significantly higher. The threshold shows sharp increases in intermediate directions between two crystal axes. At such directions the threshold is limited by replacements outside the spheres of third neighbors. In some other cases the knock-on can displace one neighbor and replace another. A di-vacancy is thus created. Preliminary results indicate that this occurs most easily if the two crystal axes involved have a relatively small angle between them, as in the case of the $\langle 110 \rangle$ and $\langle 111 \rangle$.

6) As a result of the directional dependence of the threshold energy, the integrated probability of displacement is a slowly rising function of knock-on energy, in contrast to the step-function forms often used. For the energy range (> 35 eV) where comparison is valid, there is reasonable agreement between the calculated displacement probability vs. energy curve and Lucasson and Walker's best-fitting "staircase" function.

7) The calculations indicate that, at knock-on energies lower than 35 eV, damage is due primarily to the formation of defects by $\langle 100 \rangle$ replacement sequences, and the displacement probability is considerably less than one. Bombardments of single crystals of α-iron with electrons below 300 keV are needed to show to what extent the predicted large differences in the damage in different orientations are real. Such experiments could also provide valuable information concerning the interatomic potential at the separations of interest to threshold events.

6. ACKNOWLEDGMENTS

The programming of these calculations has been under the capable supervision of Mrs. R. E. Larsen. Contributions have also been made by M. Milgram. Helpful discussions, particularly on the static problems, with R. A. Johnson are gratefully acknowledged, and thanks are extended to A. A. Abrahamson for his work on interatomic potentials.

References

1. G. H. Vineyard, J. B. Gibson, A. N. Goland and M. Milgram, Bull. Am. Phys. Soc. II, 5, 26 (1960); J. B. Gibson, A. N. Goland, M. Milgram and G. H. Vineyard, Phys. Rev. 120, 1229 (1960).

2. G. H. Vineyard, Strengthening Mechanisms in Solids, American Society for Metals, Cleveland (1960).

3. G. H. Vineyard, Proc. International School of Physics "Enrico Fermi" XVIII Course, Academic Press, New York (1962), pp. 291-317.

4. G. H. Vineyard, Energia Nucleare 8, 9 (1961).

5. G. H. Vineyard and J. B. Gibson, Bull. Am. Phys. Soc. II, 6, 158 (1961).

6. G. H. Vineyard, Disc. Faraday Soc. 31, 7 (1961).

7. G. H. Vineyard, B. Mozer and A. N. Goland, Bull. Am. Phys. Soc. II, 7, 170 (1962).

8. C. Erginsoy and G. H. Vineyard, Bull. Am. Phys. Soc. II, 8, 196 (1963).

9. G. H. Vineyard, J. Phys. Soc. Japan, 18, Supp. III, 144 (1963).

10. P. G. Lucasson and R. M. Walker, Disc. Faraday Soc. 31, 57 (1961); Phys. Rev. 127, 485 (1962).

11. B. J. Alder and T. Wainwright, J. Chem. Phys. 27, 1208 (1957); ibid 31, 349 (1959); ibid 33, 1439 (1960); Phys. Rev. 127, 359 (1962).

12. L. A. Girifalco and V. G. Weizer, Phys. Rev. 114, 687 (1959).

13. C. Erginsoy, Proc. ASTM Symposium on the Chemical and Physical Effects of High Energy Irradiation on Inorganic Substances, 1963 (to be published).

14. O. B. Firsov, Soviet Physics JETP, 6 (33), 534 (1958).

References (continued)

15. A. Abrahamson, R. D. Hatcher and G. H. Vineyard, Phys. Rev. 121, 159 (1961).

16. A. Abrahamson, Phys. Rev. 130, 693 (1963).

17. R. Silsbee, J. Appl. Phys. 28, 1246 (1957); G. Leibfried, ibid 30, 1388 (1959).

18. R. S. Nelson, Phil. Mag. 8, 693 (1963).

19. A. Lucasson, P. Lucasson and R. M. Walker, International Conference on the Properties of Reactor Materials and the Effects of Radiation Damage, Butterworths (1962).

20. P. G. Lucasson (private communication).

Figure Captions

Fig. 1 Interatomic potentials for a pair of iron atoms as a function of their separation r. Most of the detailed work reported was done with Potential III.

Fig. 2 Potential II and III at the larger separations. r_o is the equilibrium separation of nearest neighbors in the crystal (r_o = 2.48 angstroms), a is the cube side (a = 2.86 angstroms), r_c is the cut-off separation for present machine calculations.

Fig. 3 Configuration of the split interstitial in the α-iron model with Potential III. Atoms in the {110} plane containing the interstitial are shown. Dotted contours denote the original positions of the atoms in the perfect lattice and the full spheres correspond to their relaxed positions.

Fig. 4 Orbits of atoms in a dynamic event initiated by a 60 eV knock-on directed at 25° to [100] in the (001) plane. The knock-on (0) makes a replacement at a third neighbor site (C) and a chain of replacement proceeds in [010].

Fig. 5 Orbits of atoms in a dynamic event initiated by a 65 eV knock-on directed at 25° to [001] in $(1\bar{1}0)$ plane. Focused chains are seen to proceed from the replaced second neighbor (A') in addition to a long replacement chain which will lead to the interstitial.

Fig. 6 Formation of a di-vacancy. The knock-on (at 0) makes a replacement at the site of a third neighbor (C) after a displacement collision with a nearest neighbor (B). Two vacancies are created (at 0 and B). One interstitial is seen at D, the other is expected to form beyond E.

Fig. 7 Diagrams showing the different barrier planes influencing dynamic replacement chains along the main crystal axes. K denotes the knock-on, $S_1, S_2, \ldots$ are the first, second, etc. struck atoms in the chain. Neighbors forming the barriers are shown by $A_{1,2} \ldots$ and $B_{1,2} \ldots$

Fig. 8 The attenuation of ⟨111⟩ pulses with time. The pulses have shock-wave velocities (1-2 x 10^6 cm/sec.) and transfer kinetic energy with little loss over long distances in the crystal. Note the initial kinetic energy drop which supplies the potential energy required to propagate the pulse.

Fig. 9 The attenuation of ⟨100⟩ pulses initiated at different angles to the chain axis.

Fig. 10 Correlated replacement sequences initiated by a 100 eV knock-on at 1^o to [110]. Replacement sequences start in [110] and defocusing causes a change of direction to [010]. Only one defect is made.

Fig. 11 Focusing parameter $\Lambda(E)$ as a function of energy E for a ⟨111⟩ chain. The limiting energy for focusing is about 28 eV.

Fig. 12 Focusing parameter $\Lambda(E)$ as a function of E for a ⟨100⟩ chain. The lower curve refers to an actual ⟨100⟩ row within the b.c.c. lattice and the upper curve to an isolated row of atoms with same spacing but with no neighbors outside the row. Focusing is seen to be due to the action of the neighbors. The limiting energy for focusing is 18 eV.

Fig. 13 Diagram showing the pattern of replacements by the knock-on at near-threshold energies. The knock-on replaces a nearest neighbor, second neighbor or a third neighbor depending on its initial direction.

Fig. 14 Directional dependence of the displacement threshold energy. Each dot shows results of a machine calculation with Potential III. The direction of easiest displacement is ⟨110⟩, giving a minimum threshold of $\sim$ 17 eV in our model. Thresholds in ⟨110⟩ and ⟨111⟩ are $\sim$ 34 eV and $\sim$ 38 eV, respectively. Note the sharp increases of the threshold between the low-index directions and the highly asymmetrical angular region in which ⟨110⟩-type replacements are possible.

Fig. 15 Contours of constant displacement threshold in the fundamental triangle bounded by the ⟨100⟩, ⟨110⟩, and ⟨111⟩ directions. The azimuthal and polar angles φ and θ define the original knock-on direction.

Fig. 16 The integrated displacement probability $P_d(E)$ for a knock-on of energy E and random direction. Contributions of three low-index directions are shown separately. Note the complexities caused by the directional dependence of the threshold. The "staircase" function of Lucasson and Walker, which gave a good fit to their experimental data on electron-irradiated α-iron is shown for comparison.

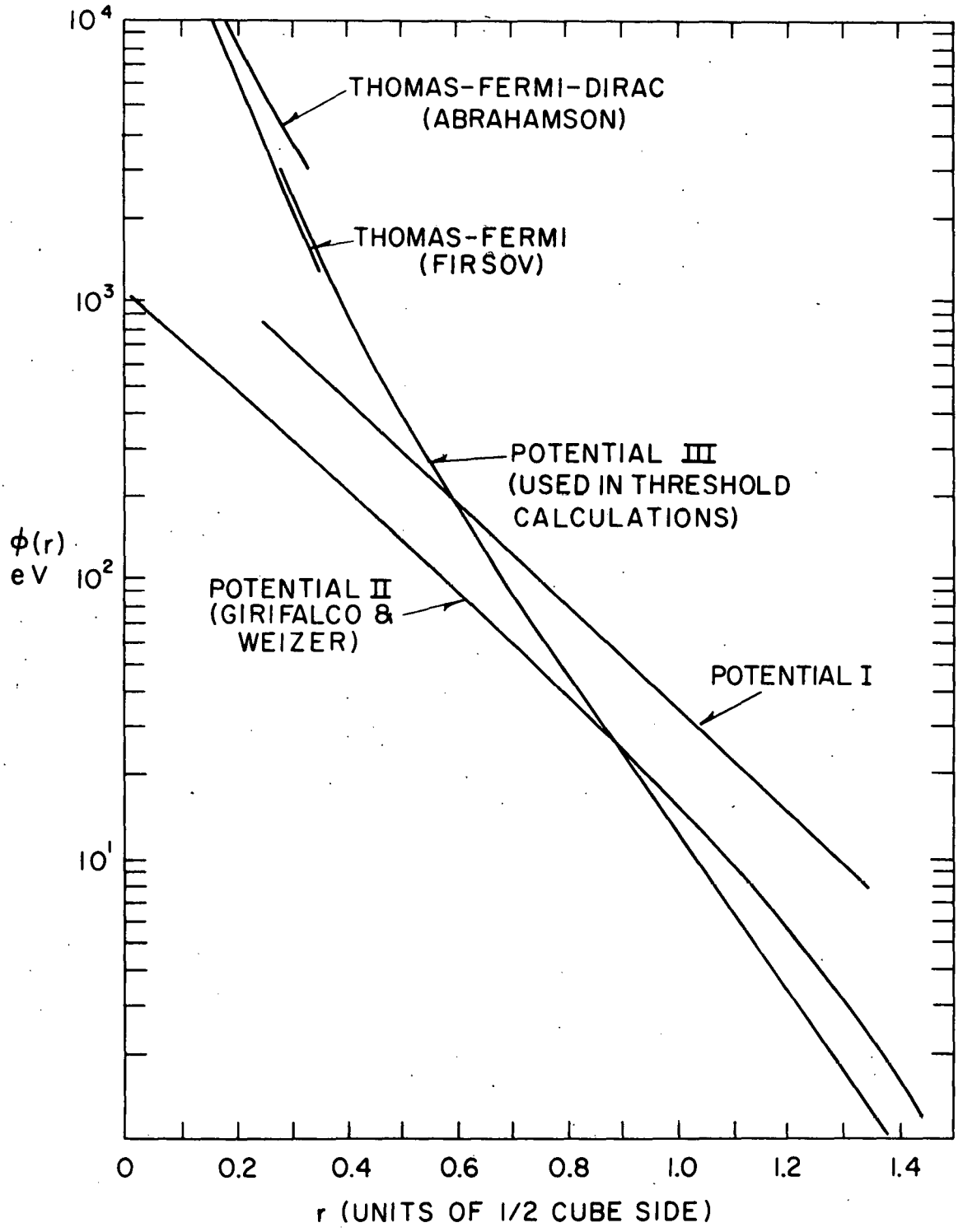
10^4
10^3
10^2
10^1
$\phi(r)$
eV
THOMAS-FERMI-DIRAC
(ABRAHAMSON)
THOMAS-FERMI
(FIRSOV)
POTENTIAL III
(USED IN THRESHOLD
CALCULATIONS)
POTENTIAL II
(GIRIFALCO &
WEIZER)
POTENTIAL I
0
0.2
0.4
0.6
0.8
1.0
1.2
1.4
r (UNITS OF 1/2 CUBE SIDE)

FIG. 1

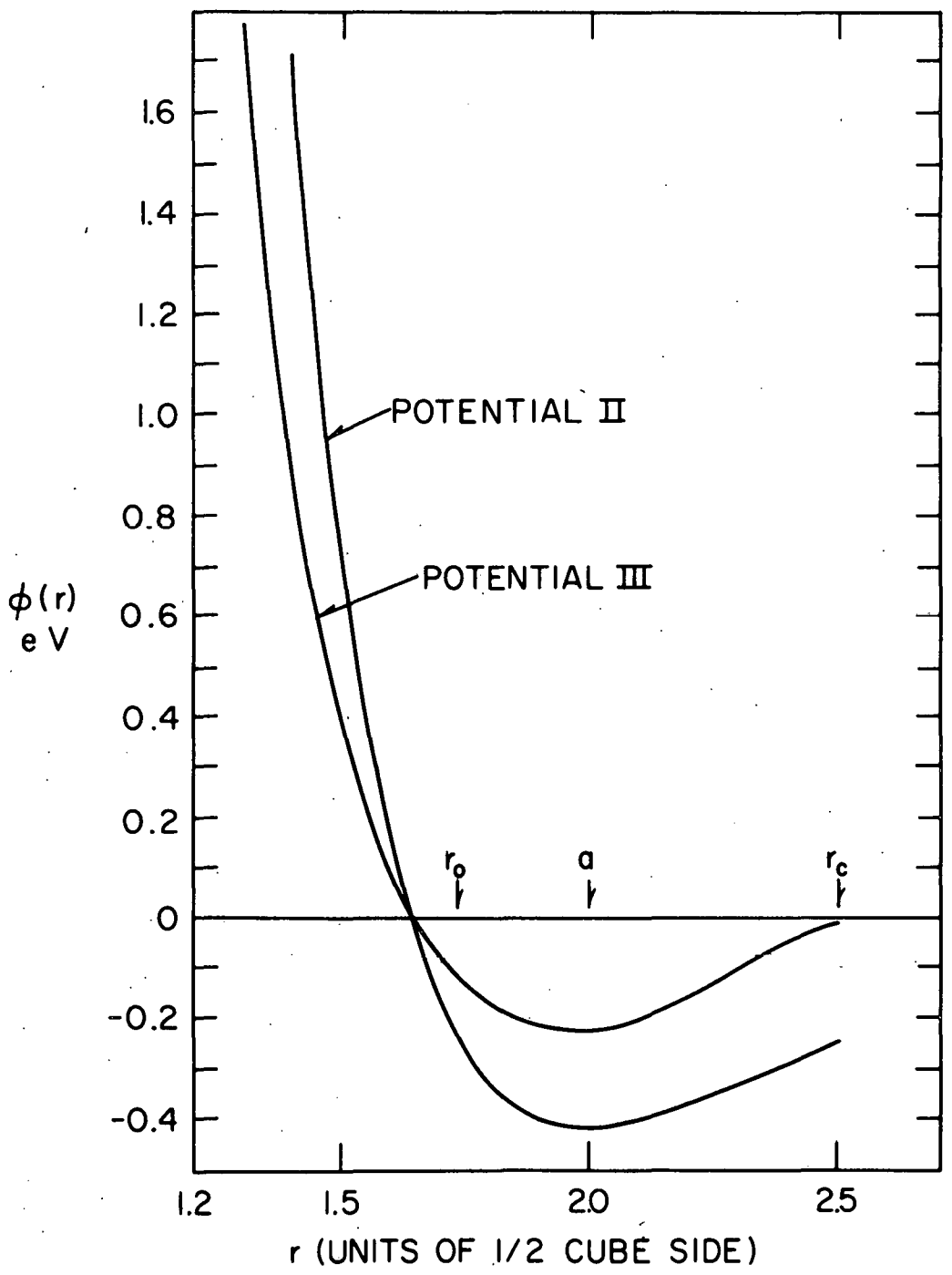
1.6
1.4
1.2
1.0
0.8
0.6
0.4
0.2
0
-0.2
-0.4
φ(r)
e V
POTENTIAL II
POTENTIAL III
r_o
a
r_c
1.2
1.5
2.0
2.5
r (UNITS OF 1/2 CUBE SIDE)

FIG. 2

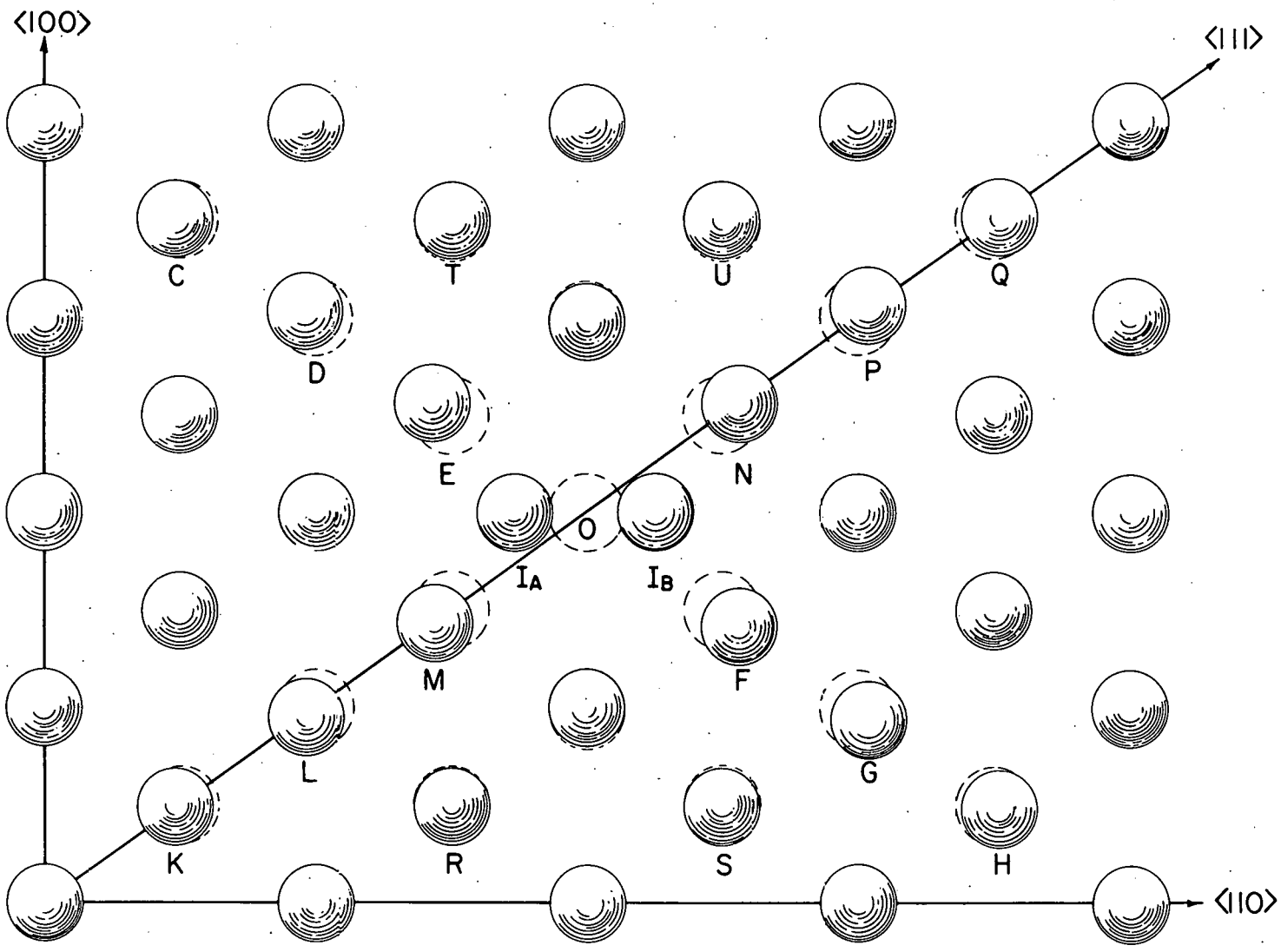

SPLIT INTERSTITIAL CONFIGURATION IN BCC LATTICE
{110} PLANE

FIG. 3

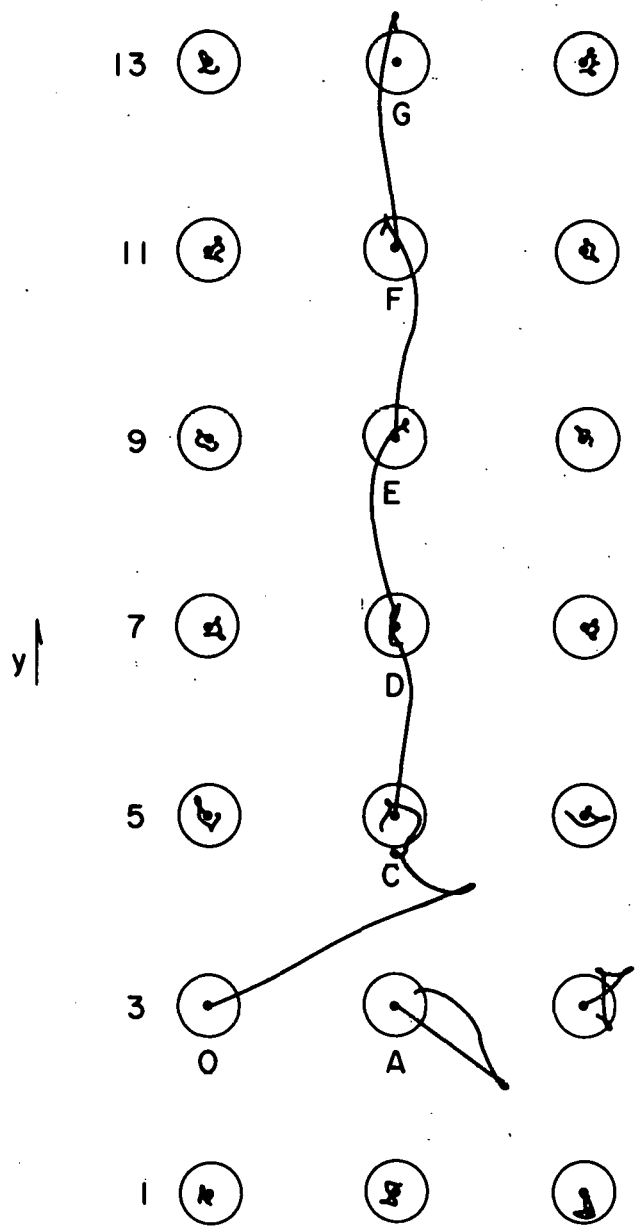

FIG. 4

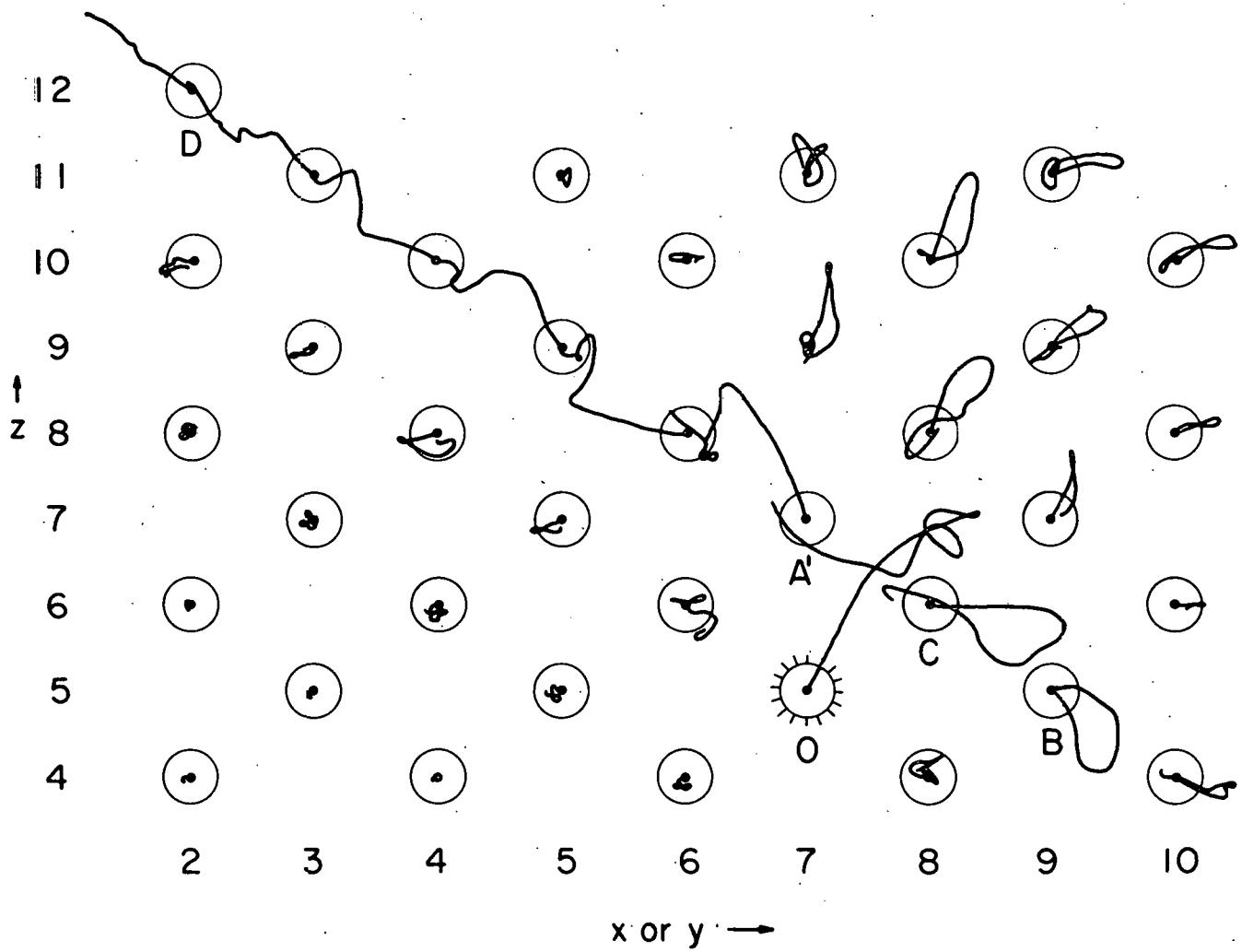

FIG. 5

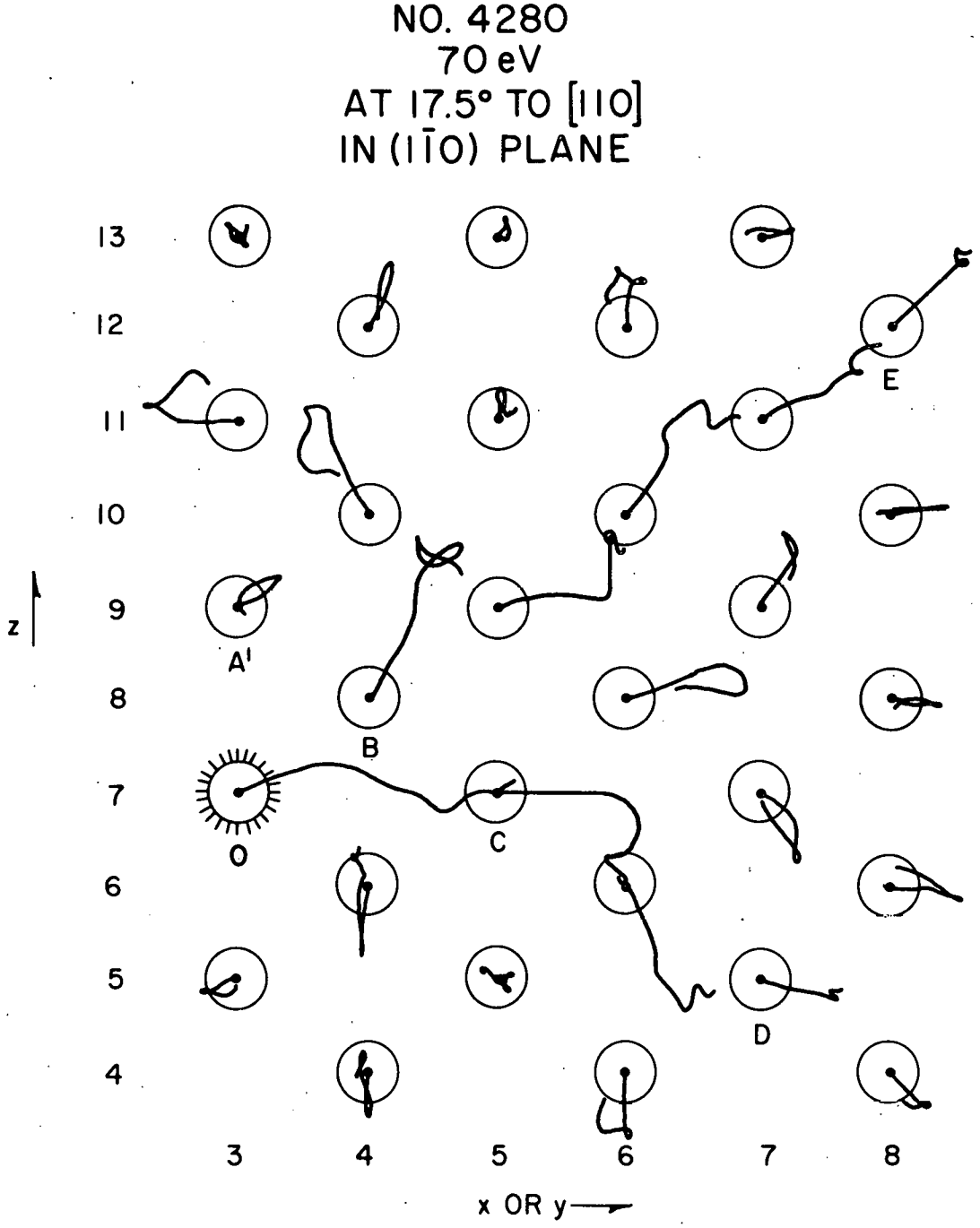
NO. 4280
70 eV
AT 17.5° TO [110]
IN (1$\bar{1}$0) PLANE
13
12
11
10
9
8
7
6
5
4
z
A'
B
C
D
E
O
3
4
5
6
7
8
x OR y

FIG. 6

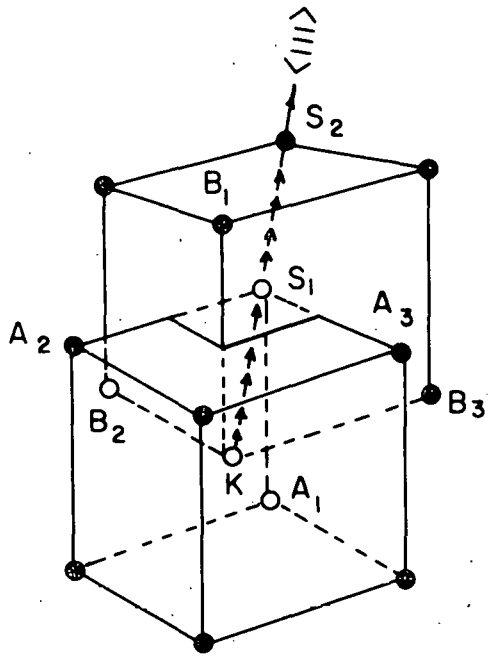

<111> COLLISION CHAIN

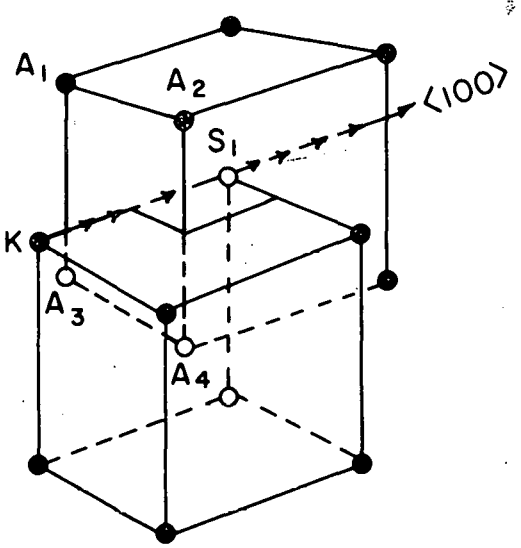

<100> COLLISION CHAIN

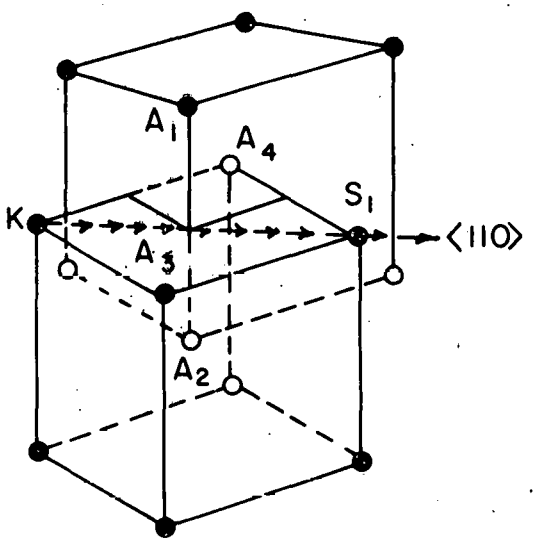

<110> COLLISION CHAIN

FIG. 7

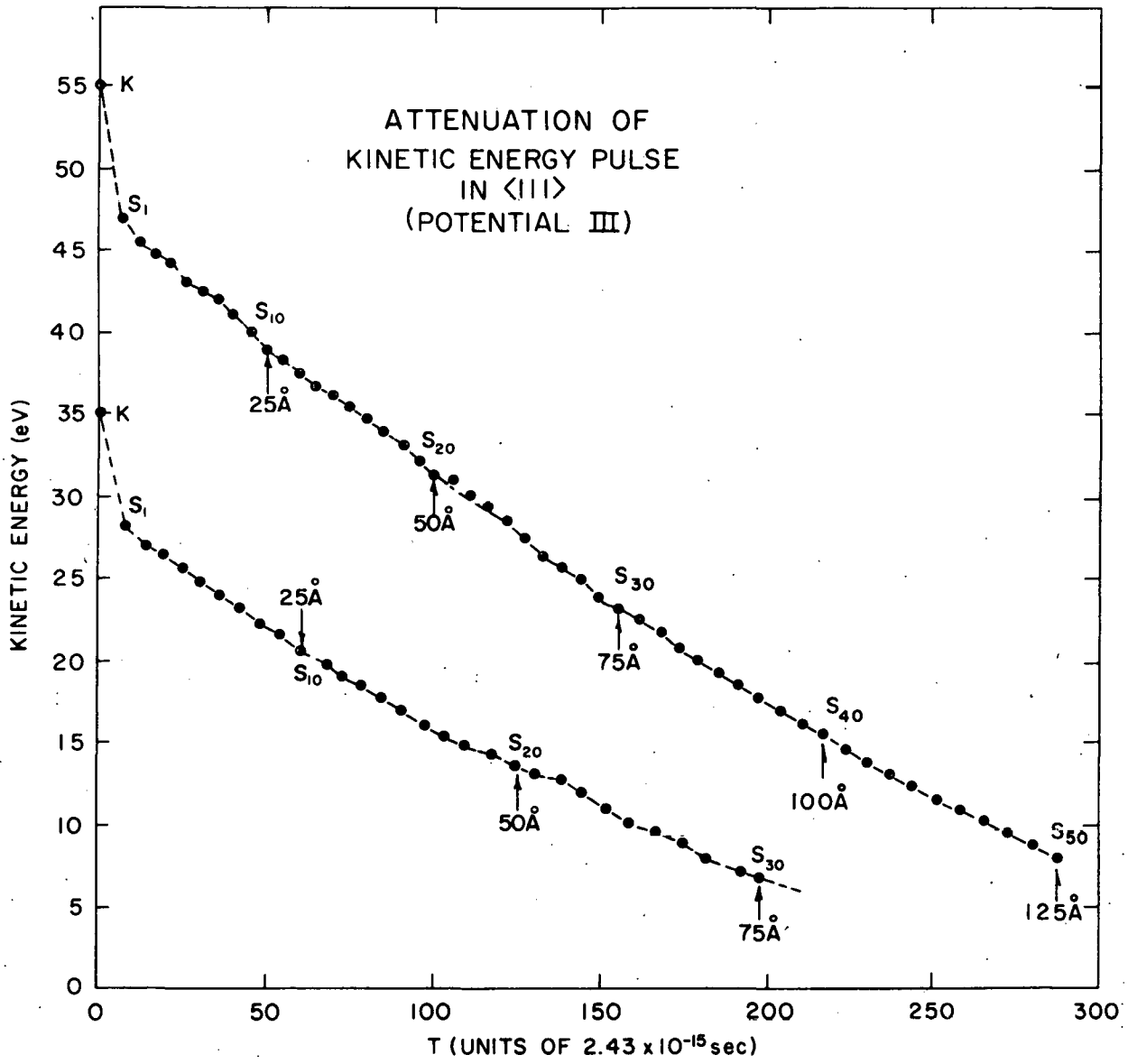
ATTENUATION OF
KINETIC ENERGY PULSE
IN ⟨111⟩
(POTENTIAL III)
KINETIC ENERGY (eV)
T (UNITS OF 2.43 x 10⁻¹⁵ sec)
K
S1
S10
S20
S30
S40
S50
25Å
50Å
75Å
100Å
125Å
0
5
10
15
20
25
30
35
40
45
50
55
0
50
100
150
200
250
300

FIG. 8

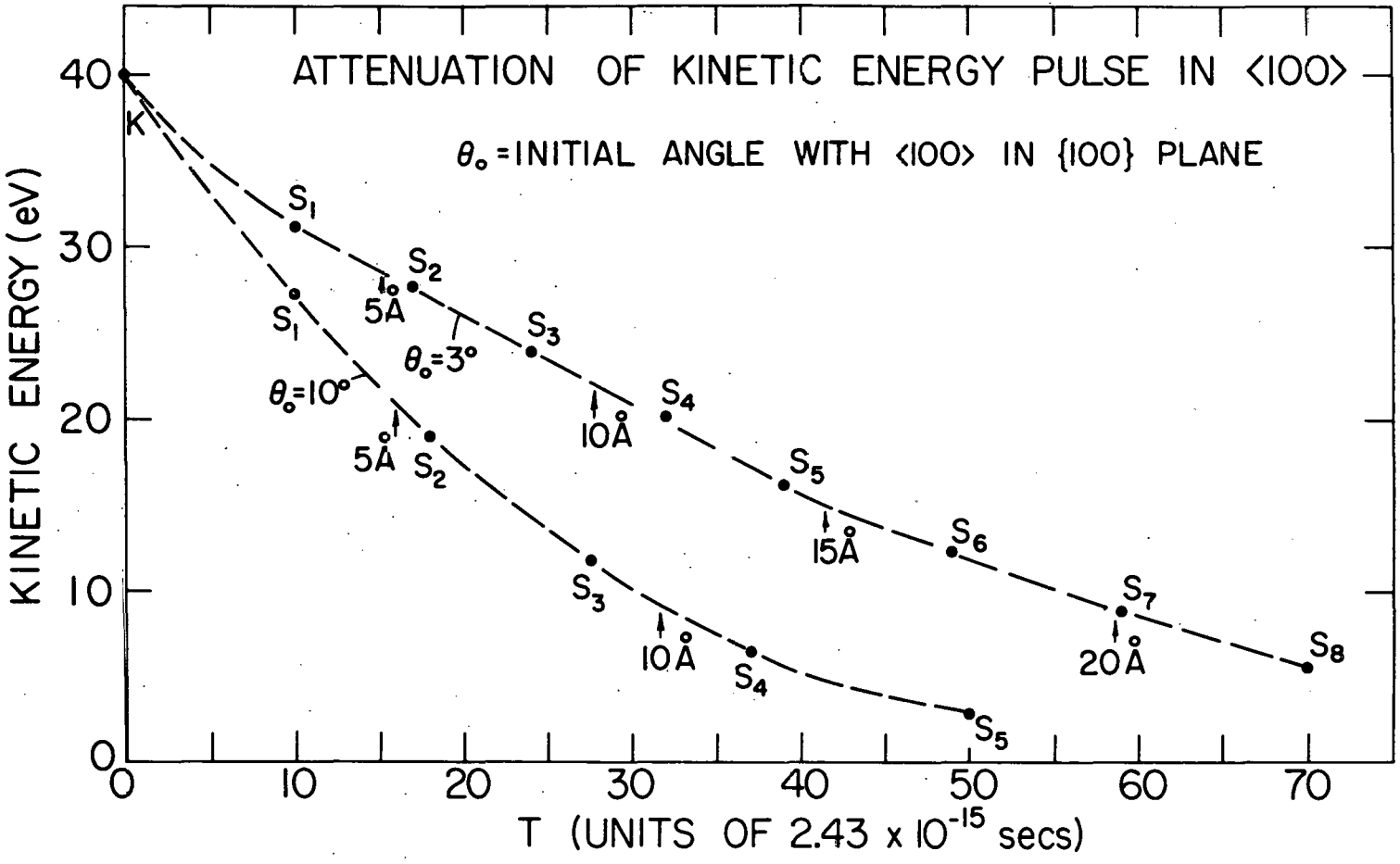
ATTENUATION OF KINETIC ENERGY PULSE IN <100>
θ₀ = INITIAL ANGLE WITH <100> IN {100} PLANE
KINETIC ENERGY (eV)
T (UNITS OF 2.43 x 10⁻¹⁵ secs)
K
S1
S2
S3
S4
S5
S6
S7
S8
5Å
10Å
15Å
20Å
θ₀=3°
θ₀=10°
0
10
20
30
40
50
60
70

FIG. 9

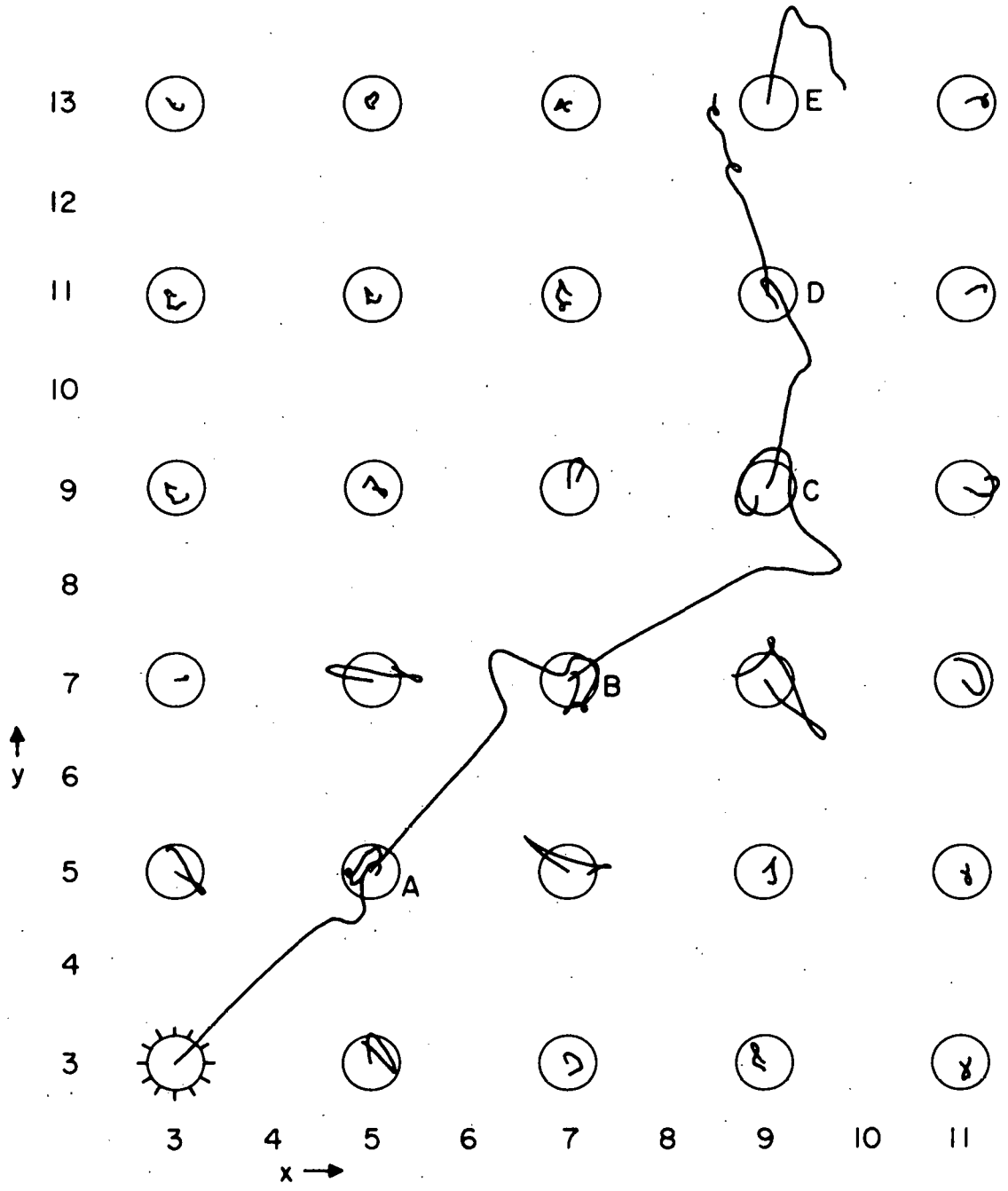

FIG. 10

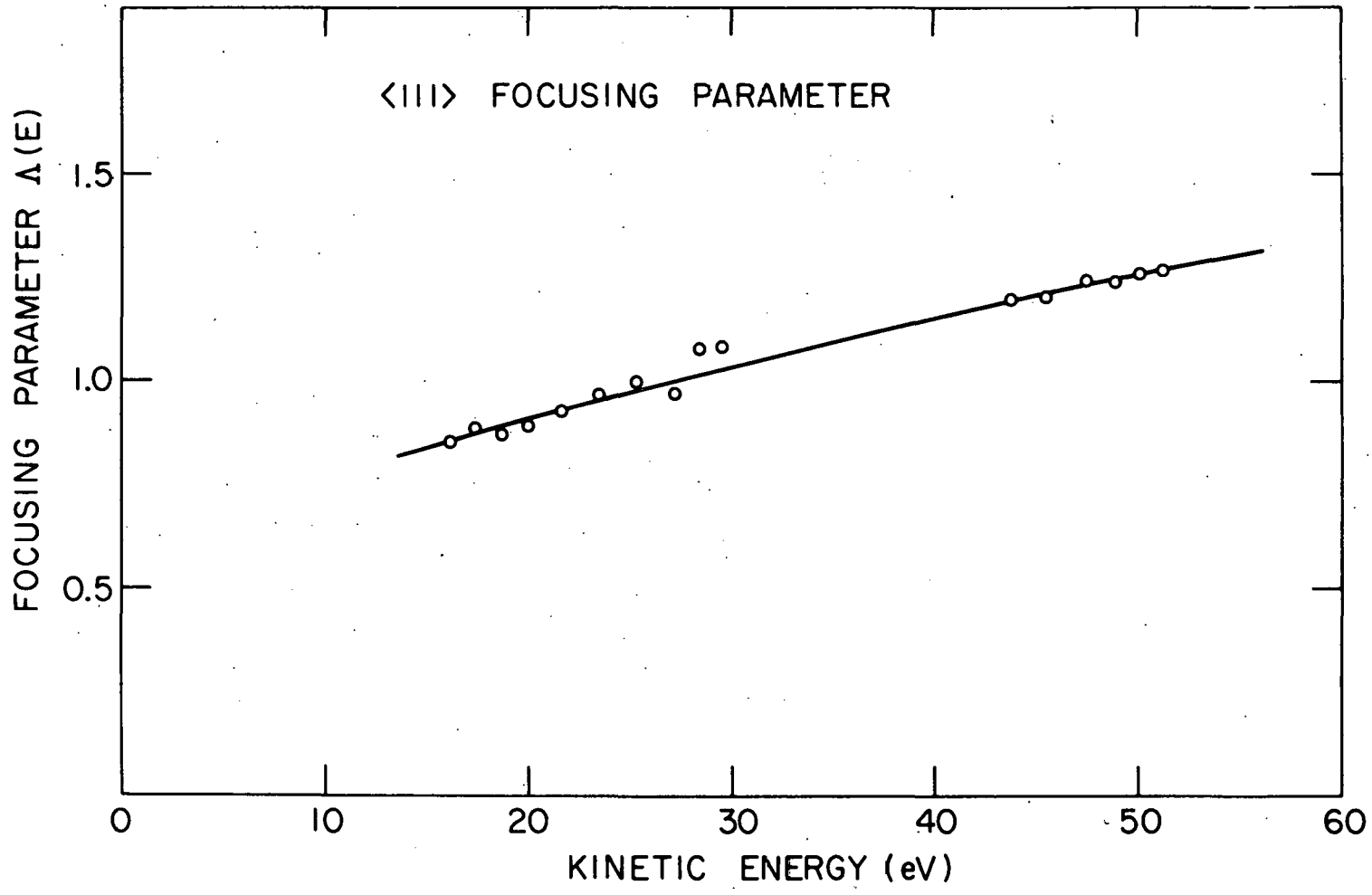
<111> FOCUSING PARAMETER
FOCUSING PARAMETER Λ(E)
1.5
1.0
0.5
0
10
20
30
40
50
60
KINETIC ENERGY (eV)

FIG. 11

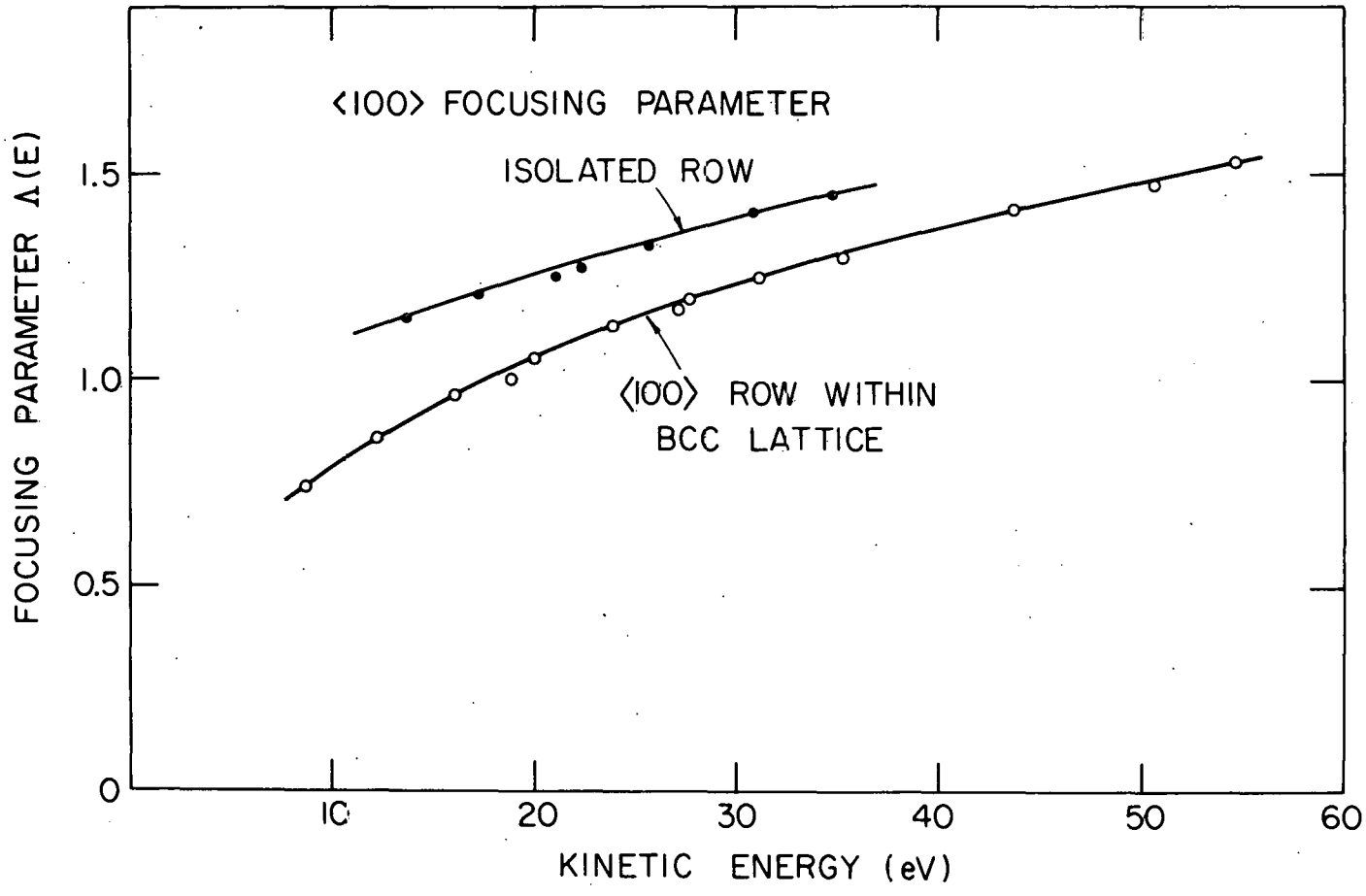
<100> FOCUSING PARAMETER
ISOLATED ROW
<100> ROW WITHIN
BCC LATTICE
FOCUSING PARAMETER Λ(E)
1.5
1.0
0.5
0
10
20
30
40
50
60
KINETIC ENERGY (eV)

FIG. 12

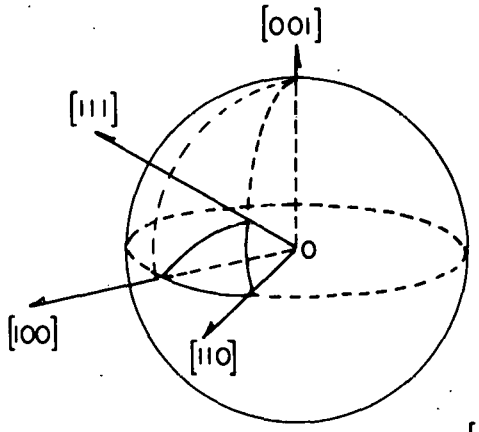

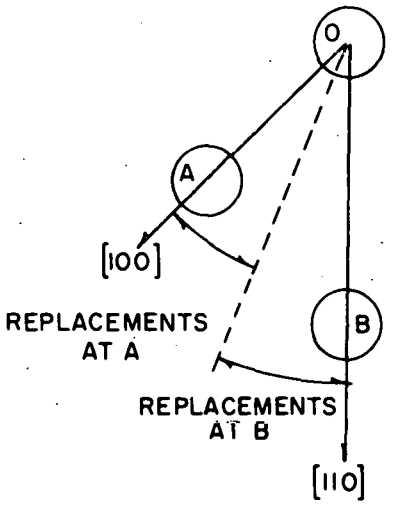

THRESHOLD REPLACEMENTS
IN {001} PLANE

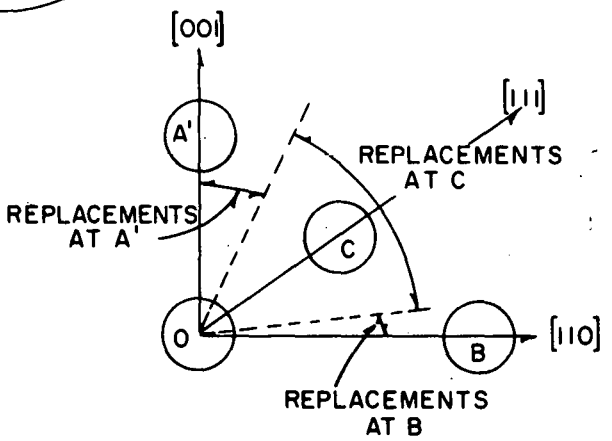

THRESHOLD REPLACEMENTS
IN {110} PLANE

FIG. 13

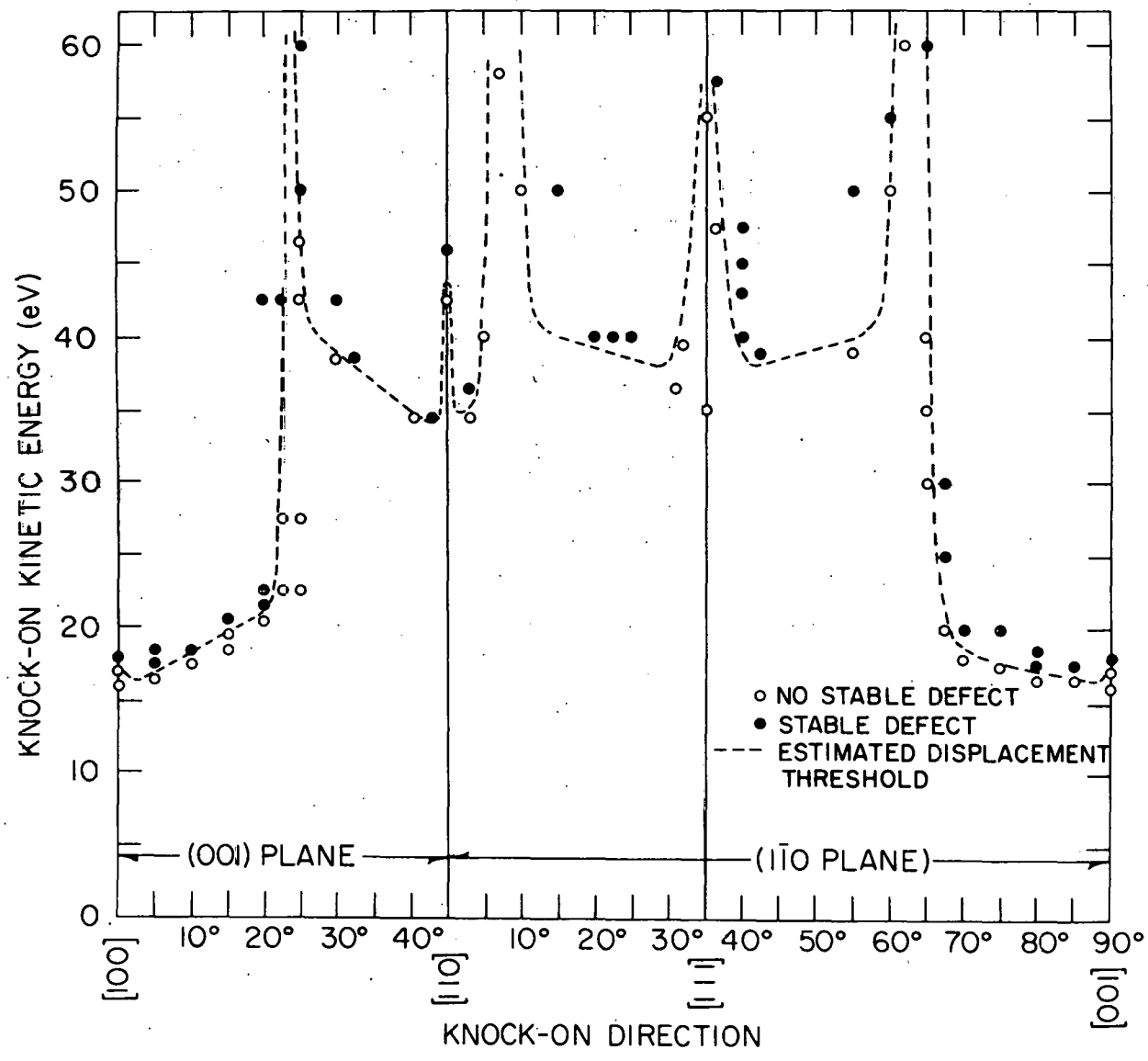
KNOCK-ON KINETIC ENERGY (eV)
60
50
40
30
20
10
0
o NO STABLE DEFECT
• STABLE DEFECT
--- ESTIMATED DISPLACEMENT THRESHOLD
(001) PLANE
(1$\bar{1}$0 PLANE)
10° 20° 30° 40°
10° 20° 30° 40° 50° 60° 70° 80° 90°
[100]
[110]
[1$\bar{1}$1]
[001]
KNOCK-ON DIRECTION

FIG. 14

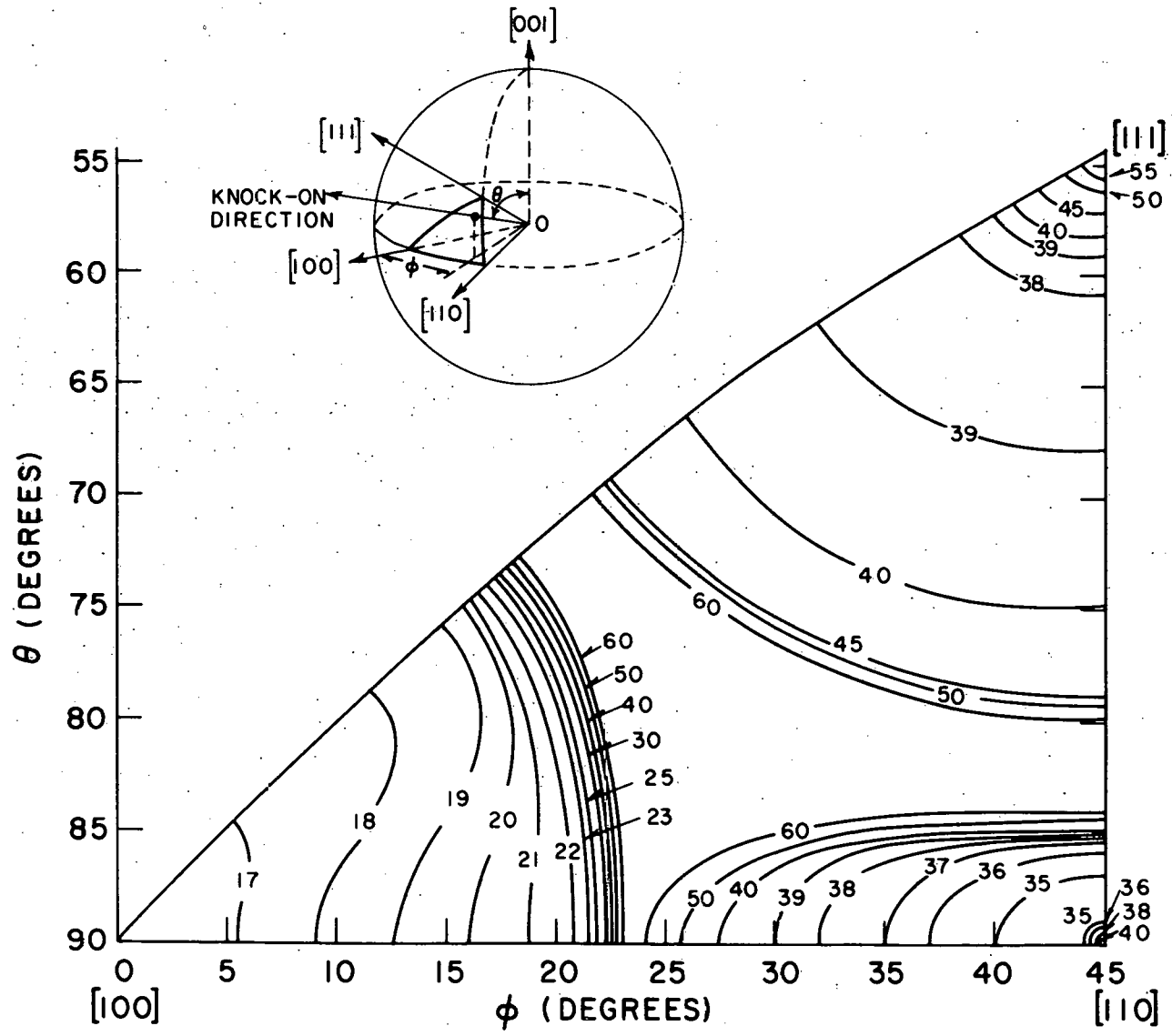
[001]
[111]
KNOCK-ON
DIRECTION
[100]
[110]
θ
φ
0
θ (DEGREES)
φ (DEGREES)
[100]
[110]
[111]
55
60
65
70
75
80
85
90
0
5
10
15
20
25
30
35
40
45
17
18
19
20
21
22
23
25
30
40
45
50
60
35
36
37
38
39

FIG. 15

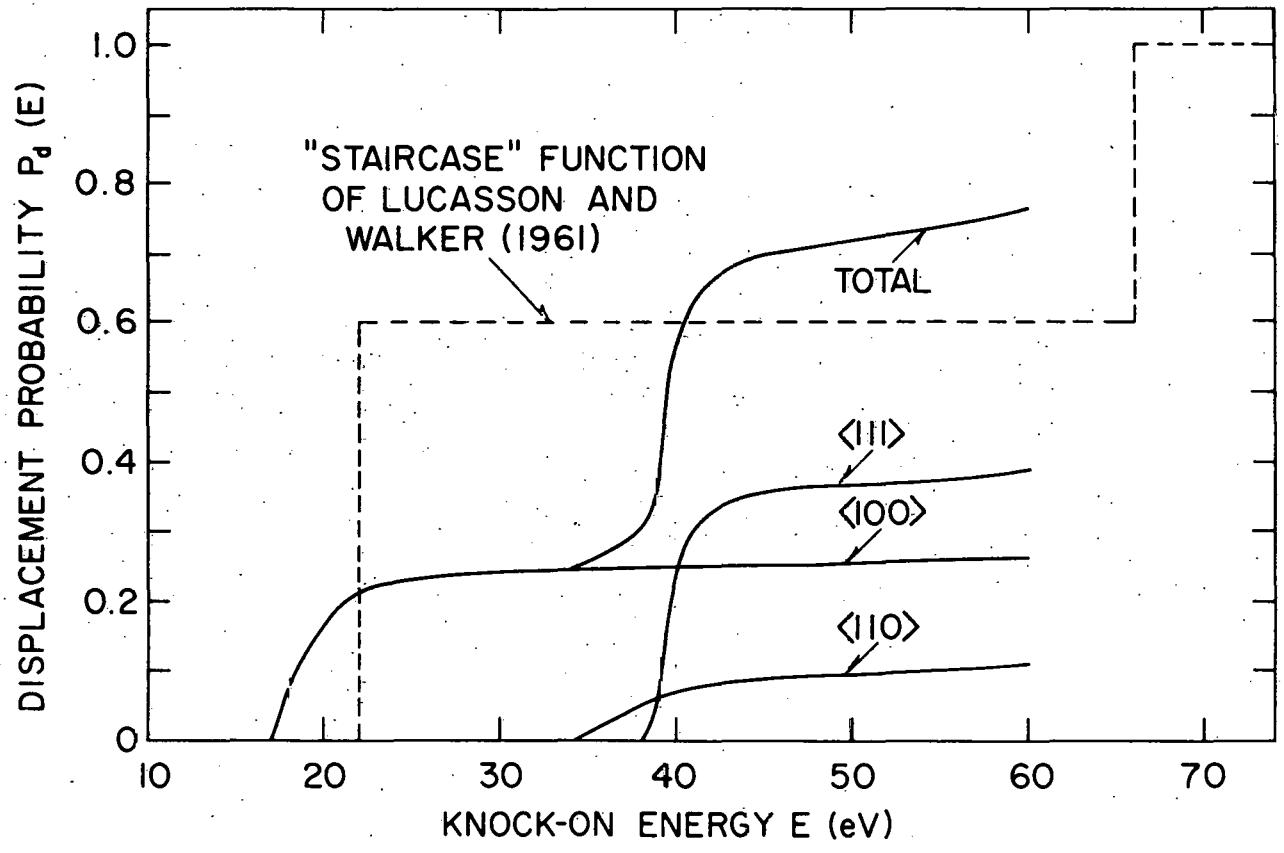
DISPLACEMENT PROBABILITY P_d (E)
1.0
0.8
0.6
0.4
0.2
0
"STAIRCASE" FUNCTION
OF LUCASSON AND
WALKER (1961)
TOTAL
⟨111⟩
⟨100⟩
⟨110⟩
10
20
30
40
50
60
70
KNOCK-ON ENERGY E (eV)

FIG. 16